ACS APPLIED MATERIALS & INTERFACES

Research Article

www.acsami.org

Robust Biomimetic-Structural Superhydrophobic Surface on Aluminum Alloy

Lingjie Li,[†,⊥] Tao Huang,[†,⊥] Jinglei Lei,*[,†] Jianxin He,[†] Linfeng Qu,[†] Peiling Huang,[†] Wei Zhou,[†] Nianbing Li,[‡] and Fusheng Pan[§]

[†]School of Chemistry and Chemical Engineering, Chongqing University, Chongqing 400044 People's Republic of China

[‡]School of Chemistry and Chemical Engineering, Southwest University, Chongqing 400715 People's Republic of China

[§]School of Materials Science and Engineering, Chongqing University, Chongqing 400044 People's Republic of China

Supporting Information

ABSTRACT: The following facile approach has been developed to prepare a biomimetic-structural superhydrophobic surface with high stabilities and strong resistances on 2024 Al alloy that are robust to harsh environments. First, a simple hydrothermal treatment in a $La(NO_3)_3$ aqueous solution was used to fabricate ginkgo-leaf like nanostructures, resulting in a superhydrophilic surface on 2024 Al. Then a low-surface-energy compound, dodecafluoroheptyl-propyl-trimethoxylsilane (Actyflon-G502), was used to modify the superhydrophilic 2024 Al, changing the surface character from superhydrophilicity to superhydrophobicity. The water contact angle (WCA) of such a superhydrophobic surface reaches up to 160°, demonstrating excellent superhydrophobicity. Moreover, the as-prepared superhydrophobic surface shows high stabilities in air-storage, chemical and thermal environments, and has strong resistances to UV irradiation, corrosion, and abrasion. The WCAs of such a surface almost remain unchanged (160°) after storage in air for 80 days, exposure in 250 °C atmosphere for 24 h, and being exposed under UV irradiation for 24 h, are more than 144° whether in acidic or alkali medium, and are more than 150° after 48 h corrosion and after abrasion under 0.98 kPa for 1000 mm length. The remarkable durability of the as-prepared superhydrophobic surface can be attributed to its stable structure and composition, which are due to the existence of lanthanum (hydr)oxides in surface layer. The robustness of the as-prepared superhydrophobic surface to harsh environments will open their much wider applications. The fabricating approach for such robust superhydrophobic surface can be easily extended to other metals and alloys.

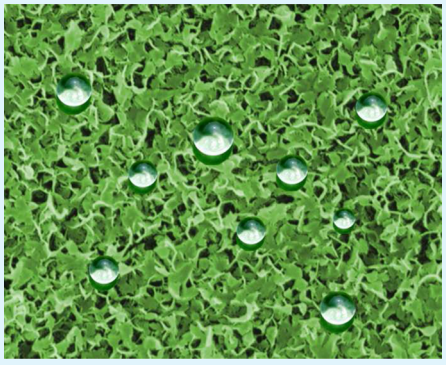

KEYWORDS: *superhydrophobic surface, biomimetic structure, aluminum alloy, hydrothermal method, durability*

1. INTRODUCTION

Aluminum alloys, especially the high-strength aluminum alloys (e.g., 2024 Al and 7075 Al, etc.), possess many excellent properties, such as remarkable high-specific strength, excellent heat, relatively low-specific weight and so on, which have many applications in many fields.[1−3] However, aluminum alloys are chemically reactive and liable to suffer severe damage during service in harsh environments, which seriously limits their applications.[3] Surface treatments are hence indispensable for improving performance and elongating service-life of aluminum alloys. Among various surface coatings of aluminum alloys, superhydrophobic surfaces with a water contact angle (WCA) greater than 150° have attracted significant attention due to their comprehensive superiority and remarkable properties (e.g., self-cleaning, anticontamination, anti-icing, antiwearing, anticorrosion, etc.), which are regarded as one of the most promising surface treatments for aluminum alloys.[4−9] However, superhydrophobic surfaces are apt to deteriorate in environments (e.g., long-term air-exposure, chemical etching, heat, irradiation, corrosion, abrasion, etc.), which seriously baffles their widespread applicability.[10−13] Therefore, durable superhydrophobic surfaces that are robust to harsh environments are highly desired for a broad range of applications of aluminum alloys, and developing the facile preparing methods for such surfaces is urgent.

Rare-earth conversion coatings have been known as green and effective surface treatments to improve corrosion resistance of aluminum alloys.[10,14−18] Moreover, the intrinsical hydrophobicity of rare-earth oxides has been currently reported.[19] Such featured wettability is attributed to the unique electronic structure of rare-earth elements, which inhibits hydrogen bonding with interfacial water molecules. Rare-earth oxides have been demonstrated to sustain hydrophobicity even after exposure to harsh environments, which suggests that rare-earth oxides may find widespread applicability as robust (super)-hydrophobic surfaces. Hence, fabricating superhydrophobic surfaces containing rare-earth oxides may pave the way to prepare durable superhydrophobic surfaces that are robust to

Received: August 20, 2014
Accepted: December 29, 2014
Published: December 29, 2014

DOI: 10.1021/am505582j
ACS Appl. Mater. Interfaces 2015, 7, 1449−1457

environments. However, to the best of our knowledge, at present there are no reports on the fabrication and robustness of the superhydrophobic surface containing rare-earth oxides.

Among the numerous methods for fabricating superhydrophobic surface,[20−29] the hydrothermal method is considered as an attractive way for its facile operating process and lack of need for sophisticated instrumentation.[29] The hydrothermal treatment can construct micro- and nanostructures on a surface, which is crucial for achieving surface superhydrophobicity.[4,29] As reported, H_2O and H_2O_2 were used as hydrothermal reaction media for creating micro- and nanostructures of (hydr)oxides on a metal surface.[4,29,30] However, there has been no exploitation to use rare-earth salt solutions as hydrothermal media to construct micro- and nanostructures and further to fabricate a superhydrophobic surface with robustness.

In the present work, a biomimetic-structural superhydrophobic surface containing lanthanum (hydr)oxides with high stabilities and strong resistances on 2024 Al alloy that are robust to environments is prepared by hydrothermally treating the 2024 Al alloy in a $La(NO_3)_3$ aqueous solution to construct ginkgo-leaf-like nanostructures containing lanthanum (hydr)oxides and then modifying the surface with a low-surface-energy compound (Actyflon-G502) to realize superhydrophobicity. The wettability, morphology, and composition of the as-prepared samples are characterized and their durability whether in air-storage, or exposure to various harsh environments (e.g., acidic/alkali, high temperature, UV irradiation, corrosion, and abrasion) are systematically studied. Moreover, the formation mechanism of the 2014 Al surfaces with special wettability is discussed, and the mechanism behind the remarkable durability of the superhydrophobic samples is explained. To the best of our knowledge, up to now, it is the first report on the biomimetic-structural superhydrophobic surface containing lanthanum (hydr)oxides with such remarkable robustness to harsh environments, and also the surface with ginkgo-leaf-like nanostructures is constructed by a hydrothermal treatment in a rare-earth salt solution for the first time.

2. EXPERIMENTAL DETAILS

2.1. Materials and Chemicals. 2024 Al alloy (Rong Chuang Metal Co., Ltd., Dongguan, PR China; composition: 92.81 wt % aluminum, 5.51 wt % copper, and 1.68 wt % magnesium) with a working area of 1.0 cm^2 was used as the substrate. Chemicals, including lanthanum nitrate ($La(NO_3)_3{\cdot}6H_2O$; Sinopharm Chemical Reagent Co., Ltd., Shanghai, PR China; analytical grade), dodecafluoroheptyl-propyl-trimethoxylsilane (Actyflon-G502; Xuejia Fluorinesilicon Chemical Co., Ltd., Harbin, PR China; chemical grade), sodium chloride (Sinopharm Chemical Reagent Co., Ltd., Shanghai, PR China; analytical grade), and ethanol (Sinopharm Chemical Reagent Co., Ltd., Shanghai, PR China; analytical grade), were used as received.

2.2. Sample Preparation. The biomimetic-structural superhydrophobic surface was prepared by the following procedures: The 2024 Al substrates were abraded with 200, 400, 800# grit emery papers, then degreased ultrasonically in absolute ethanol for 5 min and rinsed with pure water. These cleaned 2024 Al substrates were promptly introduced into a Teflon-lined stainless steel autoclave (with 45 mL space) that was filled with 15 mL 0.001 M $La(NO_3)_3$ aqueous solution. The autoclave was then sealed with a lid and maintained at 120 °C for 3 h and subsequently left to cool to room temperature. Then the 2024 Al samples were removed and dried in air. Subsequently, the 2024 Al samples were immersed in a mixed solution of ethanol (14.8 mL) and Actyflon-G502 (0.2 mL) for 24 h and finally heated at 160 °C for 1 h. For expression convenience, the sample after hydrothermal treatment in a $La(NO_3)_3$ aqueous solution was abridged as LHTS and that further after modification with Actyflon-G502 was abridged as MLHTS.

For comparison, some related control samples were present. The water-hydrothermal sample was abridged as WHTS, which was prepared under identical conditions of LHTS except the hydrothermal reaction medium was pure water (in the absence of $La(NO_3)_3$). WHTS further after modification with Actyflon-G502 was abridged as MWHTS. The blank sample was abridged as BS, which was actually a cleaned 2024 Al substrate only undergoing the identical pretreatments of LHTS and WHTS.

2.3. Surface Characterization. The sample surface morphology was characterized using a focused ion beam scanning electron microscope (FIB-SEM, Zeiss Auriga, Germany). The surface chemical composition was analyzed by X-ray photoelectron spectroscopy (XPS, Thermoelectron ESCALAB 250, USA). The infrared spectra of the samples were investigated by using Fourier transform infrared spectrometry (FTIR, Nicolet iN10, USA). The surface wettability was evaluated by water-contact-angle measurements (WCA, Dataphysics OCA20, Germany) under static condition.

2.4. Resistance and Stability Tests. The corrosion, UV, and abrasion resistances of the samples were respectively examined by immersing the samples in a 3.5 wt % NaCl corrosive medium, exposing the samples under UV irradiation (irradiated by a UV light at 254 nm wavelength), and a scratch test that was previously reported[31,32] (the detailed test process is described in S1 and the corresponding schematics is illustrated in Figure S1 of the Supporting Information). The long-term air-storage, chemical, and thermal stabilities of the samples were respectively estimated by storing the samples in air for months and recording the evolution of WCAs upon air-storage, measuring the WCAs by dropping an aqueous solution droplet with different pH values (ranging from 1 to 14), and exposing the samples in 250 °C atmosphere for 24 h and recording the evolution of WCAs upon exposure. Each test was repeated three times to verify reproducibility of the results. All tests except that for thermal stability were conducted at room temperature.

3. Results and Discussion. **3.1. Surface Wettability and Morphology.** Figure 1 illustrates the water droplet (2 μL) shapes on different sample surfaces. The BS surface shows a static WCA of ca. 36° (Figure 1a), indicating the hydrophilic nature of 2024 Al. The WHTS and LHTS surfaces show WCAs of ca. 3° (Figure 1b) and 0° (Figure 1 c), respectively, indicating the formation of superhydrophilic surfaces after hydrothermal treatments whether in pure water or in a $La(NO_3)_3$ aqueous solution. After further modification with Actyflon-G502, the MWHTS surface has a static WCA of ca. 142° (Figure 1d), indicating a hydrophobic character, while the MLHTS surface exhibits a superhydrophobic character with a static WCA of ca. 160° (Figure

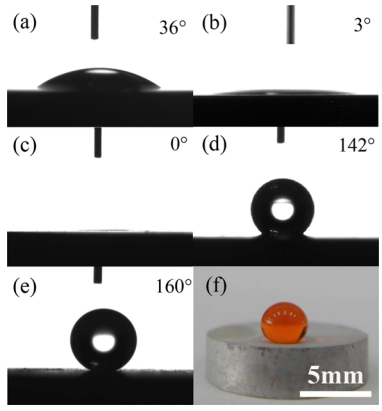

Figure 1. Digital photographs of water droplet (2 μL) shapes on different sample surfaces: (a) BS, (b) WHTS, (c) LHTS, (d) MWHTS and (e) MLHTS. (f) Digital photo of a water droplet on the as-prepared MLHTS surface.

DOI: 10.1021/am505582j
ACS Appl. Mater. Interfaces 2015, 7, 1449−1457

1e). A water droplet remains as a sphere on the as-prepared MLHTS surface (Figure 1f).

Figure 2 presents typical FIB-SEM images of the above BS, WHTS, LHTS, and MLHTS surfaces. The BS surface (Figure 2a) is flat, where

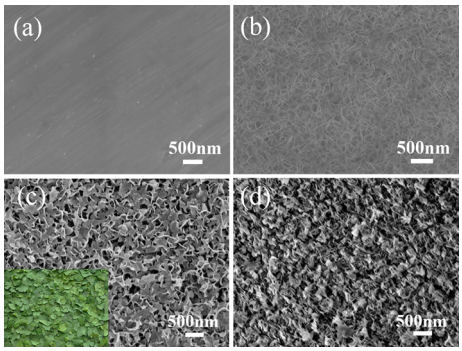

Figure 2. FIB-SEM images of different sample surfaces: (a) BS, (b) WHTS, (c) LHTS (inset: digital photo of ginkgo leaves) and (d) MLHTS.

no micro- or nanostructures can be observed. Figure 2b shows the FIB-SEM image of WHTS surface, which is covered with random-stacked nanowhiskers. The LHTS surface (Figure 2c) is uniformly covered with interesting ginkgo-leaf-like (inset of Figure 2c) structures with thicknesses of 10−30 nm and diameters of 100−300 nm. The FIB-SEM image of the MLHTS superhydrophobic surface (Figure 2d) indicates that the modification process with Actyflon-G502 has no remarkable impact on the surface morphology.

From the above results, it can be deduced that the fabricating method proposed here, employing a hydrothermal treatment in a $La(NO_3)_3$ aqueous solution to create a rough surface with a biomimetic structure, and further modifying the surface with a low-surface-energy compound (Actyflon-G502), is an effective way to prepare superhydrophobic surface and change the surface wetting characteristic from superhydrophilic and superhydrophobic.

3.2. Surface Composition. Figure 3 shows XPS results of the above BS, WHTS, and LHTS surfaces. From the survey spectra (Figure 3a), the elements Al, O, and C (contamination from air) are detected at the BS and WHTS surfaces, which confirms that the BS surface is covered with a native oxide film and the WHTS surface consists of aluminum (hydr)oxides formed during the hydrothermal process.[30] For the LHTS surface, the elements Al, La, O, and C (contamination from air) are examined. The high-resolution spectra of Al 2p, La 3d, and O 1s for the LHTS surface are further illustrated in Figure 3b−d. The Al 2p high-resolution spectrum (Figure 3b) can be resolved into two components with binding energies of 73.7 and 75.7 eV. The strong peak at 73.7 eV is assigned to AlOOH and the weak one at 75.7 eV is assigned to Al_2O_3.[33,34] The La 3d high-resolution spectrum (Figure 3c) shows two major peaks at 835.4 and 852.2 eV (with a spin-energy separation of 16.8 eV), respectively corresponding to La $3d_{5/2}$ and La $3d_{3/2}$, along with the satellite peaks at 839.1 and 855.7 eV, which are characteristic of La element in +3 valency.[35] The O 1s high-resolution spectrum (Figure 3d) can be fitted by five peaks, respectively centered at 532.0, 531.6, 530.9, 530.3 and 529.0 eV. The two components located at 532.0 and 530.9 eV are assigned to AlOOH, and the one at 530.3 eV is assigned to Al_2O_3.[36,37] The two peaks at 531.6 and 529.0 eV can be attributed to O in $La(OH)_3$ and La_2O_3, respectively.[38] Quantitative analysis of the XPS results reveals that the 2024 Al surface after the hydrothermal treatment consists of Al (32.50 at%), La (0.58 at%) and O (66.92 at%). Thus, it is inferred that the LHTS surface is essentially composed of (hydr)oxides of lanthanum and aluminum. Additionally, there are abundant hydroxyls and small amounts of adsorbed H_2O existing at the surface, which can be deduced from the FTIR results (Figure S2 and corresponding discussion).

Figure 4 shows XPS results of the MWHTS and MLHTS surfaces. From the survey spectra (Figure 4a), the elements F, C, Si, and O were introduced during the modification process for both surfaces and the chemical composition difference of the two surfaces is the La element in the MLHTS surface that induced during the hydrothermal process. The MWHTS surface is deduced to consist of only aluminum (hydr)oxide and modified compounds. The high-resolution spectra of F 1s, C 1s, Si 2p, O 1s, Al 2p and La 3d for the MLHTS surface are further illustrated in Figure 4b−g. The F 1s high-resolution spectrum at 688.9 eV (Figure 4b) is correlated with C−F bonds.[39] The C 1s high-resolution spectrum (Figure 4c) can be fitted by six peaks respectively centered at 293.8, 289.9, 289.0, 286.4, 284.9, and 284.6 eV, which can be assigned to $-CF_3$, $-CF_2$, $-CH_2-CF_2$, −C−C, −C−O or the contaminated C during storage, and −C−Si.[39,40] The Si 2p

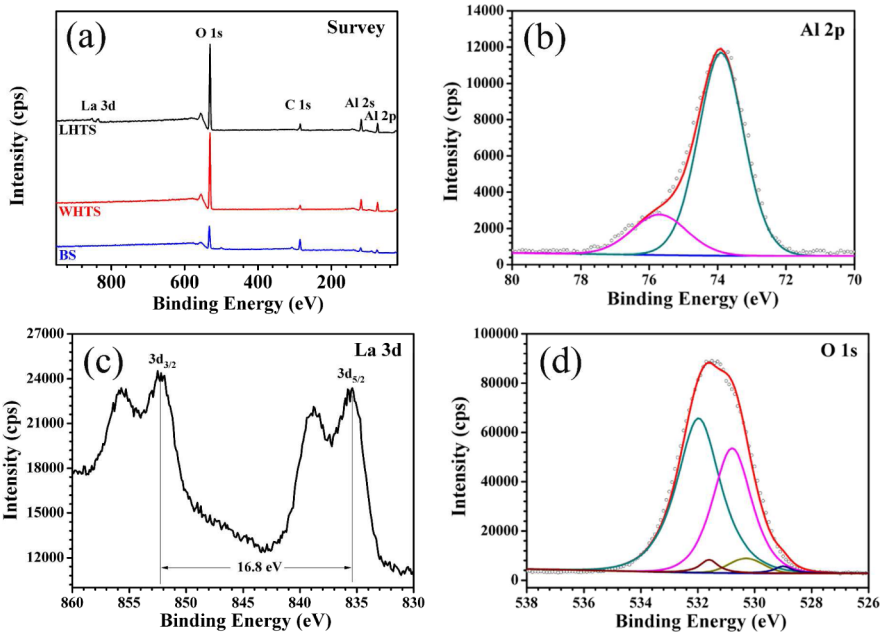

Figure 3. (a) XPS survey spectra of BS, WHTS, and LHTS surfaces; and XPS high-resolution spectra of LHTS surface: (b) Al 2p, (c) La 3d, and (d) O 1s.

DOI: 10.1021/am505582j
ACS Appl. Mater. Interfaces 2015, 7, 1449−1457

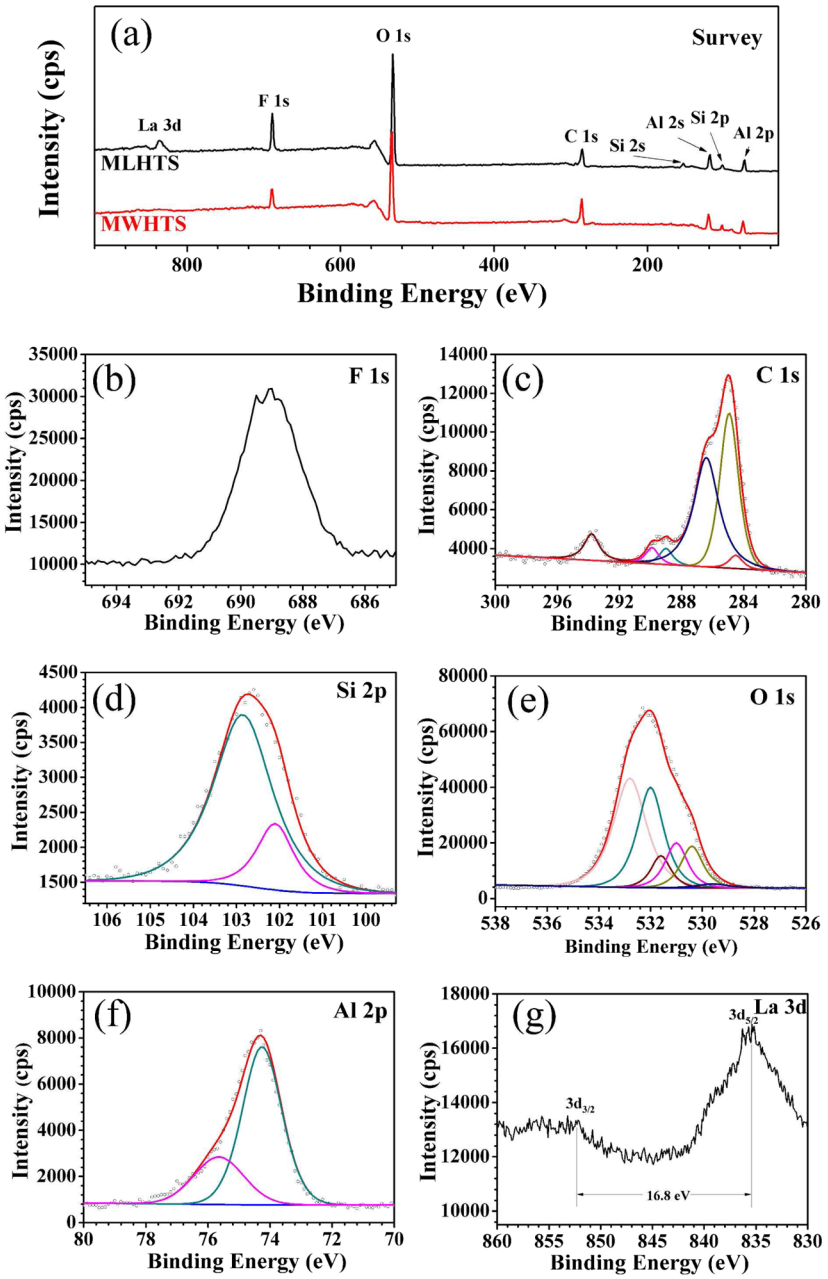

Figure 4. (a) XPS survey spectra of MLHTS and MWHTS surfaces. XPS high-resolution spectra of MLHTS surface: (b) F 1s, (c) C 1s, (d) Si 2p, (e) O 1s, (f) Al 2p, and (g) La 3d.

peak (Figure 4d) can be resolved into two components with binding energies of 102.9 and 102.1 eV, which can be assigned to Si−O and Si−C bonding, respectively.[36] The O 1s peak (Figure 4e) can be resolved into six components with the binding energies of 532.8, 532.0, 531.6, 530.9, 530.3, and 529.0 eV. The component located at 532.8 eV is usually attributed to the presence of a −Si−O bond.[41] The component located at 532.0, 531.6, 530.9, 530.3, and 529.0 eV can be correlated with (hydr)oxides of lanthanum and aluminum at the sample surface.[36−38] In addition, the Al 2p and La 3d spectra (Figure 4f,g) show similar binding energies but much lower intensities, as compared with those of the unmodified sample (Figure 3b,c), which indicates that the modified layer is ultrathin and part of the (hydr)oxides underlayer can be detected. Quantitative analysis of the XPS results reveals that the MLHTS surface essentially consists of F (8.49 at. %), C (22.07 at. %), Si (5.79 at. %), O (43.37 at. %), Al (20.1 at. %), and La (0.18 at. %). Thus, it can be deduced that during the modification process the interfacial polymerization reactions occurred between the silanol groups and surface hydroxyl groups to form $C_{10}F_{12}H_9Si(O\text{-surface})_3$, which covers the sample surface and endows it with superhydrophobicity.[42]

3.3. Resistances and Stabilities. The corrosion resistance of a surface layer on a high-strength aluminum alloy is crucial for its application, so first the corrosion resistance of the BS, MWHTS and MLHTS surfaces on 2024 Al are evaluated by immersing the samples into a 3.5 wt % NaCl corrosive medium. Figure 5a shows the evolution of WCAs of three different surfaces upon immersion. The WCA of the BS surface decreases from ca. 36° to 11° during 48h immersion and that of the MWHTS surface decreases from ca. 142° to 26°, while that of the MLHTS surface decreases to ca. 155° after immersion for 1 h and then almost keeps constant between 1 and 48 h with WCA of ca. 150°. Figure 5b shows the digital photos of the BS, MWHTS and MLHTS surfaces after immersion in the NaCl corrosive medium for 48 h. The serious damages are observed on the BS surface, and some small pits are densely distributed on the MWHTS surface, while the MLHTS surface shows little change. These results indicate that the as-prepared MLHTS surface has much stronger corrosion resistance to

DOI: 10.1021/am505582j
ACS Appl. Mater. Interfaces 2015, 7, 1449−1457

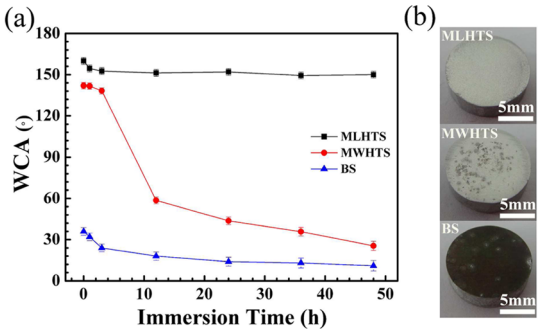

Figure 5. (a) Evolution of WCAs of BS, MWHTS, and MLHTS surfaces upon immersion in a 3.5 wt % NaCl corrosive medium. (b) Digital photos of BS, MWHTS, and MLHTS surfaces after immersion in a 3.5 wt % NaCl corrosive medium for 48 h.

corrosive medium than the BS and MWHTS surfaces, which is highly desired in the application of high-strength aluminum alloys. Moreover, these results confirm the necessity of the hydrothermal treatment in a $La(NO_3)_3$ aqueous solution for the remarkable corrosion resistance of the as-prepared MLHTS superhydrophobic surface and the crucial role of lanthanum (hydr)oxides in the surface layer for the excellent durability in corrosive environment.

Because the BS and MWHTS surfaces exhibit very poor corrosion resistance and have no actual utility, only the durability of the as-prepared MLHTS superhydrophobic surfaces in various environments is studied in the following section. Figure 6 shows the durability test results of the as-prepared MLHTS superhydrophobic surface. The UV resistance was examined by exposing the sample under UV irradiation. Figure 6a shows the evolution of WCAs upon UV irradiation. The WCAs remain nearly unchanged (ca. 160°) within experimental error (±2°) during 24 h irradiation, indicating the significant resistance of the as-prepared superhydrophobic surface to UV irradiation. The abrasion resistance of the surface was examined by a scratch test. Figure 6b shows the evolution of WCAs upon dragging in one direction with a speed of 5 mm s^{-1} under 0.98 kPa pressure. The WCA slightly decreases to ca. 154° after dragging 1000 mm length. And Figure 6c displays the relationship between the applied pressure and WCAs after dragging 1000 mm length. The WCA slightly decreases with increasing the applied pressure, and when the applied pressure increases to 4.9 kPa, the WCA decreases to 147°. These results indicate that the as-prepared MLHTS superhydrophobic surface has superior abrasion resistance to other reported superhydrophobic surfaces,[32] which is very important for its practical applications. The long-term stability was estimated by storing the sample in air for

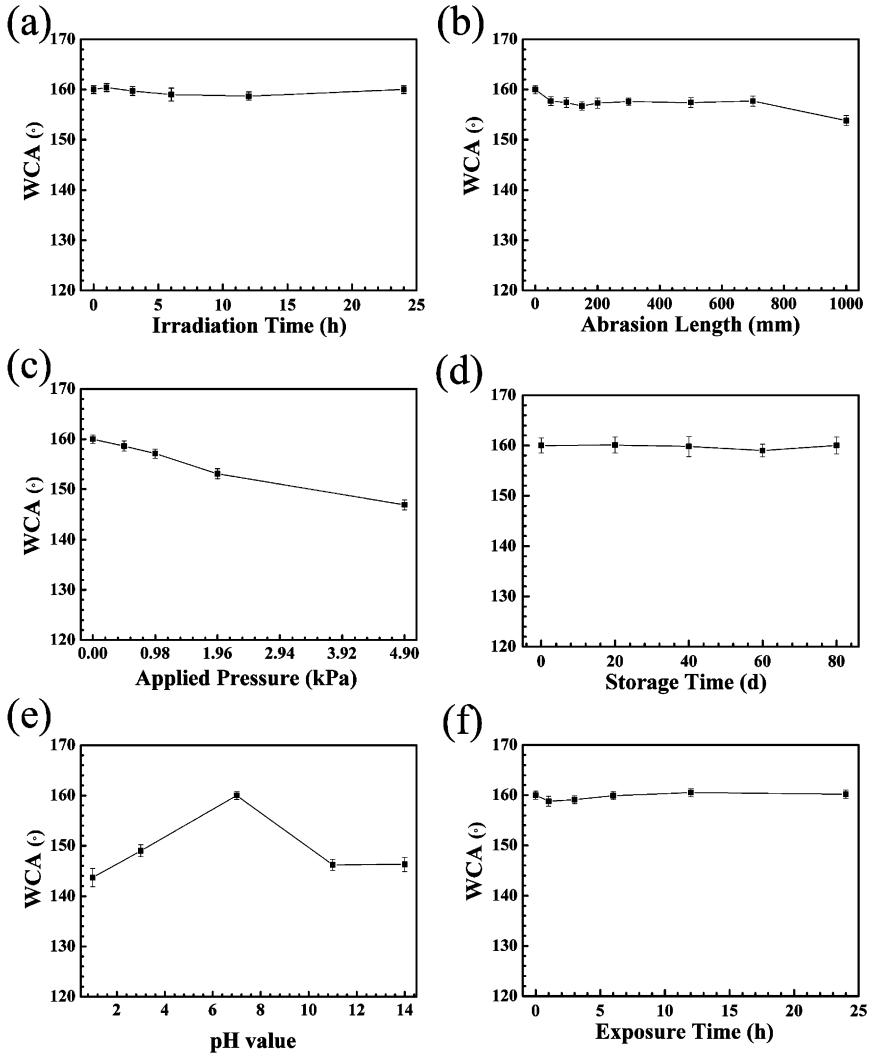

Figure 6. Evolution of WCAs of MLHTS surface upon (a) UV irradiation, (b) abrasion length under 0.98 kPa pressure, (d) storage in air, and (f) exposure in 250 °C atmosphere; Relationships between (c) the applied pressure and WCAs on MLHTS surface after dragging 1000 mm length, and (e) pH and WCAs on MLHTS surface.

DOI: 10.1021/am505582j
ACS Appl. Mater. Interfaces 2015, 7, 1449−1457

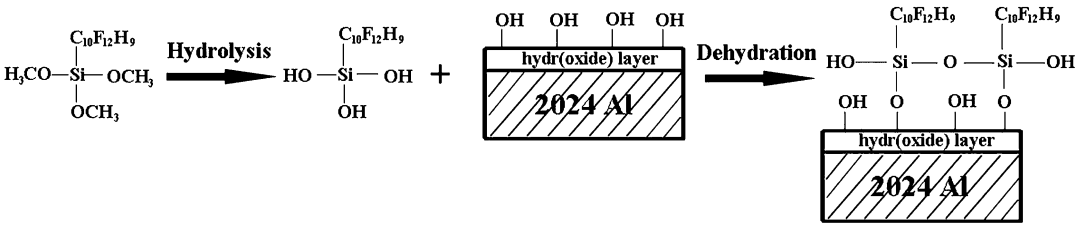

Figure 7. Schematic illustration of an Actyflon-G502 modification process.

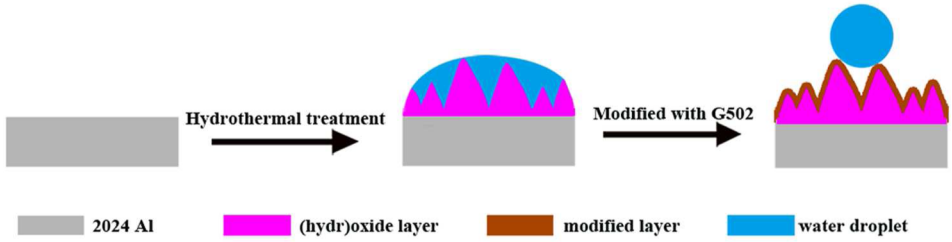

Figure 8. Schematic illustration of the fabricating process of the MLHTS superhydrophobic surface.

months. Figure 6d shows the evolution of WCAs upon storage in air. The WCAs show no decrease (ca. 160°) during air-storage for 80 days, indicating an excellent long-term stability of the as-prepared MLHTS superhydrophobic surface. The chemical stability of the surface in aqueous solutions with different pH values was examined by investigating the relationship between pH and WCAs. Figure 6e shows the relationship between pH and WCAs on the MLHTS surface. The WCAs for the most acidic medium (pH = 1) and most alkali medium (pH = 14) are respectively ca. 144° and ca. 146°. All the WCAs over the 1−14 pH range are in the range of 144° to 160°, indicating that the pH value of the aqueous solution has no remarkable effect on the surface wettability. These results indicate that the as-prepared MLHTS surface shows (super)hydrophobic property in various aqueous medium whether in neutral solutions or acidic and basic solutions. The thermal stability of the surface was tested by exposing the sample in 250 °C atmosphere for 24 h. Figure 6f shows the evolution of WCAs upon exposure in 250 °C atmosphere, which displays almost no change (ca. 160°), indicating the MLHTS surface superhydrophobicity can be maintained up to 250 °C. These results suggest that the as-prepared MLHTS superhydrophobic surface has superior thermal stability to other reported superhydrophobic surfaces.[43]

All the above experimental results on resistances and stabilities reveal that the as-prepared MLHTS superhydrophobic surface has remarkable durability whether in air-storage, or exposure to various harsh environments (e.g., corrosive medium, UV irradiation, mechanical abrasion, acidic/alkali and high-temperature), suggesting the robustness of the as-prepared surface to environments. Further consideration of the facileness of the preparation approach of such surface, it is hopeful to realize large-scale production of such durable superhydrophobic engineering materials with wide industrial applications.

3.4. Mechanisms. To put deep insight into the formation and robustness of the as-prepared MLHTS superhydrophobic surface, the corresponding mechanisms are discussed in the following sections.

3.4.1. Formation Mechanism. From the XPS results, the reactions during the hydrothermal process in a $La(NO_3)_3$ aqueous solution can be written as follows

$$H_2O(l) \rightarrow H^+(aq) + OH^-(aq) \quad (1)$$

$$2Al(s) + 6H^+(aq) \rightarrow 2Al^{3+}(aq) + 3H_2(g) \quad (2)$$

$$Al^{3+}(aq) + 3OH^-(aq) \rightarrow AlOOH(s) + H_2O(l) \quad (3)$$

$$2AlOOH(s) \rightarrow Al_2O_3(s) + H_2O(l) \quad (4)$$

$$La^{3+}(aq) + 3OH^-(aq) \rightarrow La(OH)_3(s) + H_2O(l) \quad (5)$$

$$2La(OH)_3(s) \rightarrow La_2O_3(s) + 3H_2O(l) \quad (6)$$

Under the high pressure and temperature created by the hydrothermal process, the ionization of water proceeds easily,[29,30,44] which can provide abundant H^+ and OH^-. The H^+ ions in the solution make the dissolution of Al substrate to form Al^{3+} ions, which further react with OH^- to form AlOOH and Al_2O_3. Meanwhile, the La^{3+} ions in the solution react with OH^- to form $La(OH)_3$ and La_2O_3, which is further precipitated on the 2024 Al surface. Thus, relying on the reactions between the Al substrate and the environment in the autoclave, (hydr)oxides of lanthanum and aluminum with ginkgo-leaf-like structures were created. Such complex biomimetic nanostructures and the abundant surface hydroxyls formed during the hydrothermal process facilitate to induce surface superhydrophilicity,[30] which shield the intrinsical hydrophobicity of rare-earth oxides.

The reactions during the modification process can be described as follows[29]

$$C_{10}F_{12}H_9Si(OCH_3)_3 + 3H_2O \rightarrow C_{10}F_{12}H_9Si(OH)_3 + 3CH_3OH \quad (7)$$

$$C_{10}F_{12}H_9Si(OH)_3 + 3\text{surface-OH} \rightarrow C_{10}F_{12}H_9Si(\text{O-surface})_3 + H_2O \quad (8)$$

First, hydrolysis of Actyflon-G502 molecules proceeded, during which trialkoxysilanes were hydrolyzed in the presence of a small amount of water to form silanol bonds (Si−OH). The silanols subsequently reacted with the surface hydroxyl groups to form a self-assembled $C_{10}F_{12}H_9Si(\text{O-surface})_3$ film. Meanwhile, a vertical polymerization occurred to form a grafted polysiloxane on the surface. The groups such as $-CH_2$, $-CF_2$, and $-CF_3$ on the modified surface have extremely low surface free energies, which induces surface superhydrophobicity. The above modification reactions are schematically illustrated in Figure 7.

Obviously, the hydrothermal treatment in a $La(NO_3)_3$ aqueous solution facilitates formation of a rough surface with biomimetic nanostructures and abundant surface hydroxyls, and the modification process depletes the surface hydroxyls to form a $C_{10}F_{12}H_9Si(\text{O-surface})_3$ film and dramatically reduces the surface energy, both of which are crucial for creating the superhydrophobic surface. Figure 8 schematically illustrates the fabricating process of the MLHTS superhydrophobic surface.

3.4.2. Robustness Mechanism. To have a better understanding of the robustness of the MLHTS superhydrophobic surface, the

DOI: 10.1021/am505582j
ACS Appl. Mater. Interfaces 2015, 7, 1449−1457

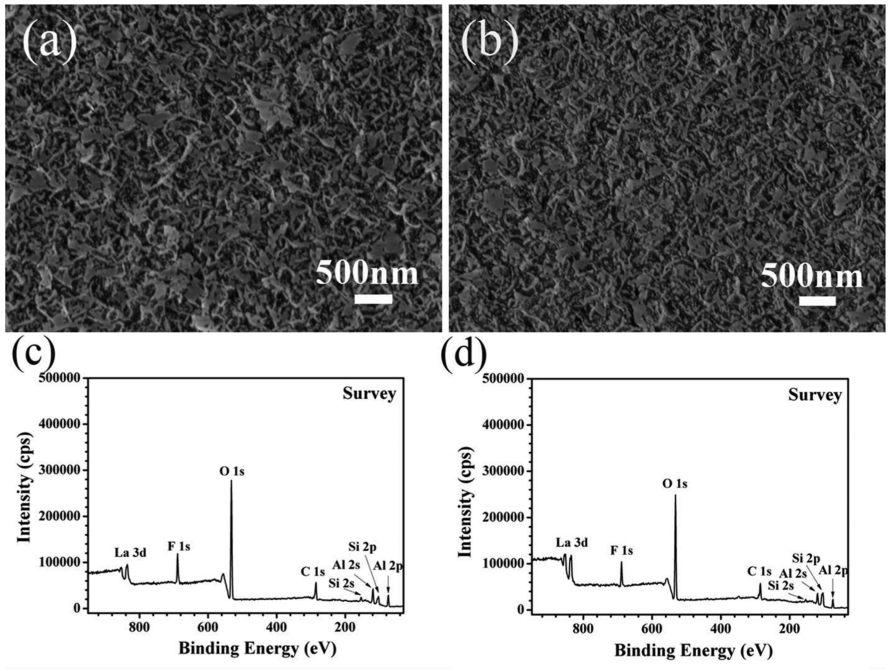

Figure 9. FIB-SEM images and XPS survey spectra of the MLHTS superhydrophobic surface after different durability tests: (a and c) 250 °C atmosphere for 24 h and (b and d) UV irradiation for 24 h.

morphology and composition of the MLHTS surface after different durability tests are characterized. Figure 9 shows the surface morphology after exposure to 250 °C atmosphere for 24 h (Figure 9a) and UV irradiation for 24 h (Figure 9b). As compared with that of the pristine sample, no obvious difference can be found, which indicates that the biomimetic nanostructures created in the hydrothermal process can sustain high stability during the stability and resistance tests. Figure 9c,d presents XPS results on the surface composition after exposure to 250 °C atmosphere for 24 h (Figure 9c) and UV irradiation for 24 h (Figure 9d). The survey spectra of those samples show little changes as compared with that of the pristine sample, which reveals that the composition of the biomimetic-structural superhydrophobic surface is highly stable in harsh environments. Hence, the remarkable durability of the as-prepared superhydrophobic surface can be attributed to its stable structure and composition. The anticorrosive and intrinsically hydrophobic characteristics of rare-earth oxides (coatings) suggest that the existence of lanthanum (hydr)oxide in 2024 Al surface layer plays a crucial role for the structural and compositional stability, which can be explained by the following two aspects.

The structural and compositional stability of the surface layer is mainly dependent on the interfacial interactions between the hydrothermal products and the low-surface energy molecules (Actyflon-G502) through the hydroxyl groups of the hydrothermal products.[4] Figure 10 schematically illustrates the bonding between $La(OH)_3$, AlOOH, and Actyflon-G502 molecules. The hydroxyl groups of $La(OH)_3$ are triple to AlOOH, which means that a $La(OH)_3$ molecule can react with three Actyflon-G502 molecules to form strong and stable bonding (Figure 10a) while an AlOOH molecule can only react with one Actyflon-G502 molecule to form relative weak bonding (Figure 10b). The strong and stable bonding between lanthanum hydroxide and Actyflon-G502 molecules is greatly helpful to sustain the structural and compositional stability of the as-prepared superhydrophobic surface layer. In addition, the intrinsical hydrophobicity of lanthanum oxide in the surface layer also benefits the robustness of the as-prepared superhydrophobic surface.[19] Figure 11 schematically illustrates the orientation of water molecules next to a La_2O_3 surface and an Al_2O_3 surface. The rare-earth lanthanum atom has a unique electronic structure with the full octet of electrons in the $5s^2p^6$ outer shell, which has a lower tendency to exchange electrons and form a hydrogen bond with interfacial water molecules, resulting in the intrinsical hydrophobicity (Figure 11a).[19,45] Whereas the aluminum atom is electron-deficient with six electrons in its three sp^2-hybrid orbitals, which tends to form a hydrogen bond with interfacial water molecules in order to achieve a full octet of electrons, resulting in the intrinsical hydrophilicity (Figure 11b).[19,46] The intrinsically hydrophobic nature of lanthanum oxide is also helpful to sustain superhydrophobicity of the as-prepared superhydrophobic surface.

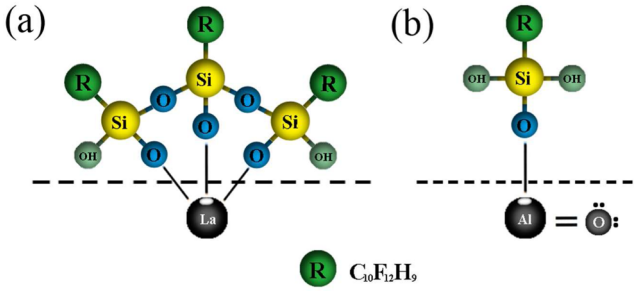

Figure 10. Schematic illustration of bonding between Actyflon-G502 and (a) $La(OH)_3$ and (b) AlOOH.

4. CONCLUSIONS

In summary, ginkgo-leaf-like nanostructures composed of (hydr)oxides of lanthanum and aluminum were constructed on a 2024 Al surface via a facile hydrothermal treatment of the sample in a $La(NO_3)_3$ aqueous solution, resulting in a superhydrophilic surface. Further modification with a low-surface-energy compound (Actyflon-G502) changed the surface wetting character from superhydrophilic to superhydrophobic (with a WCA of ca. 160°). The as-prepared superhydrophobic surface shows remarkable durability in various environments, which is due to the stable surface structure and composition for the existence of lanthanum (hydr)oxide in the surface layer. The strong and stable bonding between lanthanum hydroxide and Actyflon-G502 molecules, and the intrinsical hydrophobicity of lanthanum oxide are both helpful to sustain the

DOI: 10.1021/am505582j
ACS Appl. Mater. Interfaces 2015, 7, 1449−1457

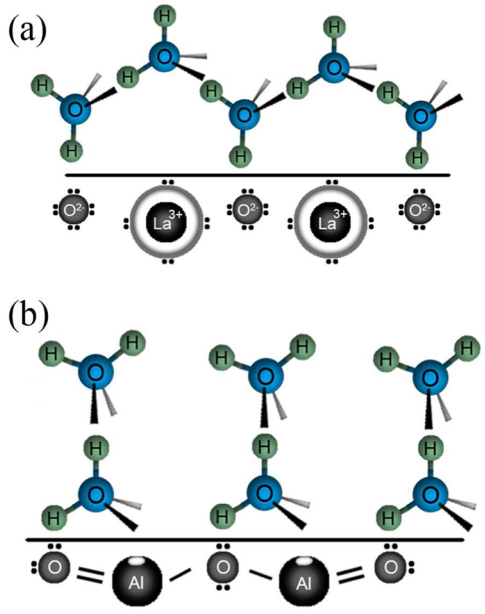

Figure 11. Schematic illustration of the orientation of water molecules next to the surface of (a) La_2O_3 and (b)Al_2O_3 (using different scales for the surface and water molecules).

structural and compositional stability of the surface layer. As the durable superhydrophobic surfaces that are robust to harsh environments are needed in a broad range of applications, the as-prepared superhydrophobic surface is expected to have widespread applicability. Moreover, the fabricating approach for such a robust superhydrophobic surface can be easily extended to other metals and alloys.

■ ASSOCIATED CONTENT

Supporting Information

Abrasion resistance test and its schematics and FTIR spectrum of the LHTS surface. This material is available free of charge via the Internet at http://pubs.acs.org.

■ AUTHOR INFORMATION

Corresponding Author

*Jinglei Lei. E-mail: JLLei@cqu.edu.cn. Tel.: +86 13983064116. Fax: +86 23 65112328.

Author Contributions

⊥Lingjie Li and Tao Huang contributed equally. The paper was written through contributions of all authors. All authors have given approval to the final version of the paper.

Notes

The authors declare no competing financial interest.

■ ACKNOWLEDGMENTS

The authors acknowledge the financial support from the National Natural Science Foundation of China (21273293, 21373281), the Natural Science Foundation of CQ (CSTC2011AB4056), the Program for New Century Excellent Talents in University (NCET-12-0587, NCET-13-0633), the Fundamental Research Funds for the Central Universities (CDJZR13225501, CDJZR14228801), the Student Research Training Program (SRTP) of Chongqing University and the sharing fund of Chongqing University's large-scale equipment.

■ REFERENCES

(1) Liu, W.; Luo, Y.; Sun, L.; Wu, R.; Jiang, H.; Liu, Y. Fabrication of the Superhydrophobic Surface on Aluminum Alloy by Anodizing and Polymeric Coating. *Appl. Surf. Sci.* **2013**, *264*, 872−878.

(2) Wang, S. C.; Starink, M. J. Two Types of S Phase Precipitates in Al−Cu−Mg Alloys. *Acta Mater.* **2007**, *55*, 933−941.

(3) Lamaka, S. V.; Zheludkevich, M. L.; Yasakau, K. A.; Montermor, M. F.; Ferreira, M. G. S. High Effective Organic Corrosion Inhibitors for 2024 Aluminium Alloy. *Electrochim. Acta* **2007**, *52*, 7231−7247.

(4) Ou, J.; Hu, W.; Xue, M.; Wang, F.; Li, W. Superhydrophobic Surfaces on Light Alloy Substrates Fabricated by a Versatile Process and Their Corrosion Protection. *ACS Appl. Mater. Interfaces* **2013**, *5*, 3101−3107.

(5) Liu, L.; Feng, X.; Guo, M. Eco-Friendly Fabrication of Superhydrophobic Bayerite Array on Al Foil via an Etching and Growth Process. *J. Phys. Chem. C* **2013**, *117*, 25519−25525.

(6) Lee, Y.; Ju, K. Y.; Lee, J. K. Stable Biomimetic Superhydrophobic Surfaces Fabricated by Polymer Replication Method from Hierarchically Structured Surfaces of Al Templates. *Langmuir* **2010**, *26*, 14103−14110.

(7) Wang, Y.; Xue, J.; Wang, Q.; Chen, Q.; Ding, J. Verification of Icephobic/Anti-icing Properties of a Superhydrophobic Surface. *ACS Appl. Mater. Interfaces* **2013**, *5*, 3370−3381.

(8) Peng, S.; Tian, D.; Yang, X.; Deng, W. Highly Efficient and Large-Scale Fabrication of Superhydrophobic Alumina Surface with Strong Stability Based on Self-Congregated Alumina Nanowires. *ACS Appl. Mater. Interfaces* **2014**, *6*, 4831−4841.

(9) Zhang, Y.; Ge, D.; Yang, S. Spray-Coating of Superhydrophobic Aluminum Alloys with Enhanced Mechanical Robustness. *J. Colloid Interface Sci.* **2014**, *423*, 101−107.

(10) Ishizaki, T.; Masuda, Y.; Sakamoto, M. Corrosion Resistance and Durability of Superhydrophobic Surface Formed on Magnesium Alloy Coated with Nanostructured Cerium Oxide Film and Fluoroalkylsilane Molecules in Corrosive NaCl Aqueous Solution. *Langmuir* **2011**, *27*, 4780−4788.

(11) Xue, C. H.; Ma, J. Z. Long-Lived Superhydrophobic Surfaces. *J. Mater. Chem. A* **2013**, *1*, 4146−4161.

(12) Liu, Y.; Liu, J.; Li, S.; Liu, J.; Han, Z.; Ren, L. Biomimetic Superhydrophobic Surface of High Adhesion Fabricated with Micro-nano Binary Structure on Aluminum Alloy. *ACS Appl. Mater. Interfaces* **2013**, *5*, 8907−8914.

(13) Ou, J.; Hu, W.; Liu, S.; Xue, M.; Wang, F.; Li, W. Superoleophobic Textured Copper Surfaces Fabricated by Chemical Etching/Oxidation and Surface Fluorination. *ACS Appl. Mater. Interfaces* **2013**, *5*, 10035−10041.

(14) Joshi, S.; Kulp, E. A.; Fahrenholtz, W. G.; O'Keefe, M. J. Dissolution of Cerium from Cerium-based Conversion Coatings on Al 7075-T6 in 0.1 M NaCl Solutions. *Corros. Sci.* **2012**, *60*, 290−295.

(15) Harvey, T. G. Cerium-based Conversion Coatings on Aluminium Alloys: A Process Review. *Corros. Eng. Sci. Technol.* **2013**, *48*, 248−269.

(16) Pardo, A.; Merino, M. C.; Arrabal, R.; Feliu, S., Jr.; Viejo, F.; Carboneras, M. Enhanced Corrosion Resistance of A3xx.x/SiCp Composites in Chloride Media by La Surface Treatments. *Electrochim. Acta* **2006**, *51*, 4367−4378.

(17) Abuin, M.; Serrano, A.; Llopis, J.; Garcia, M. A.; Carmona, N. Silica Doped with Lanthanum Sol−Gel Thin Films for Corrosion Protection. *Thin Solid Films* **2012**, *520*, 5267−5271.

(18) Li, L.; Lei, J.; Yu, S.; Tian, Y.; Jiang, Q.; Pan, F. *J.* Formation and Characterization of Cerium Conversion Coatings on Magnesium Alloy. *J. Rare Earths* **2008**, *26*, 383−387.

(19) Azimi, G.; Dhiman, R.; Kwon, H. M.; Paxson, A. T.; Varanasi, K. K. Hydrophobicity of Rare-Earth Oxide Ceramics. *Nat. Mater.* **2013**, *12*, 315−320.

(20) Yao, X.; Xu, L.; Jiang, L. Fabrication and Characterization of Superhydrophobic Surfaces with Dynamic Stability. *Adv. Funct. Mater.* **2010**, *20*, 3343−3349.

(21) Crick, C. R.; Parkin, I. P. CVD of Copper and Copper Oxide Thin Films via the in Situ Reduction of Copper (II) Nitrate—A Route

DOI: 10.1021/am505582j
ACS Appl. Mater. Interfaces 2015, 7, 1449−1457

to Conformal Superhydrophobic Coatings. *J. Mater. Chem.* **2011**, *21*, 14712−14716.
(22) Darmanin, T.; de Givenchy, E. T.; Amigoni, S.; Guittard, F. Superhydrophobic Surfaces by Electrochemical Processes. *Adv. Mater.* **2013**, *25*, 1378−1394.
(23) Li, L.; Breedveld, V.; Hess, D. W. Creation of Superhydrophobic Stainless Steel Surfaces by Acid Treatments and Hydrophobic Film Deposition. *ACS Appl. Mater. Interfaces* **2012**, *4*, 4549−4556.
(24) Xu, W.; Leeladhar, R.; Kang, Y. T.; Choi, C. H. Evaporation Kinetics of Sessile Water Droplets on Micropillared Superhydrophobic Surfaces. *Langmuir* **2013**, *29*, 6032−6041.
(25) Motlagh, N. V.; Birjandi, F. Ch.; Sargolzaei, J.; Shahtahmassebi, N. Durable, Superhydrophobic, Superoleophobic and Corrosion Resistant Coating on the Stainless Steel Surface Using a Scalable Method. *Appl. Surf. Sci.* **2013**, *283*, 636−647.
(26) Ellinas, K.; Pujari, S. P.; Dragatogiannis, D. A.; Charitidis, C. A.; Tserepi, A.; Zuilhof, H.; Gogolides, E. Plasma Micro-Nanotextured, Scratch, Water and Hexadecane Resistant, Superhydrophobic, and Superamphiphobic Polymeric Surfaces with Perfluorinated Monolayers. *ACS Appl. Mater. Interfaces* **2014**, *6*, 6510−6524.
(27) Fernandez-Blazquez, J. P.; Fell, D.; Bonaccurso, E.; del Campo, A. Superhydrophilic and Superhydrophobic Nanostructured Surfaces via Plasma Treatment. *J. Colloid Interface Sci.* **2011**, *357*, 234−238.
(28) Liu, W.; Luo, Y.; Sun, L.; Wu, R.; Jiang, H.; Liu, Y. Fabrication of the Superhydrophobic Surface on Aluminum Alloy by Anodizing and Polymeric Coating. *Appl. Surf. Sci.* **2013**, *264*, 872−878.
(29) Li, L.; Zhang, Y.; Lei, J.; He, J.; Lv, R.; Li, N.; Pan, F. A Facile Approach to Fabricate Superhydrophobic Zn Surface and Its Effect on Corrosion Resistance. *Corros. Sci.* **2014**, *85*, 174−182.
(30) Li, L.; Zhang, Y.; Lei, J.; He, J.; Lv, R.; Li, N.; Pan, F. Water-Only Hydrothermal Method: A Generalized Route for Environmentally-Benign and Cost-Effective Construction of Superhydrophilic Surfaces with Biomimetic Micronanostructures on Metals and Alloys. *Chem. Commun.* **2014**, *50*, 7416−7419.
(31) Su, F.; Yao, K. Facile Fabrication of Superhydrophobic Surface with Excellent Mechanical Abrasion and Corrosion Resistance on Copper Substrate by a Novel Method. *ACS Appl. Mater. Interfaces* **2014**, *6*, 8762−8770.
(32) She, Z.; Li, Q.; Wang, Z.; Li, L.; Chen, F.; Zhou, J. Researching the Fabrication of Anticorrosion Superhydrophobic Surface on Magnesium Alloy and Its Mechanical Stability and Durability. *Chem. Eng. J.* **2013**, *228*, 415−424.
(33) Shen, S. C.; Chen, Q.; Chow, P. S.; Tan, G. H.; Zeng, X. T.; Wang, Z.; Tan, B. H. Steam-Assisted Solid Wet-Gel Synthesis of High-Quality Nanorods of Boehmite and Alumina. *J. Phys. Chem. C* **2007**, *111*, 700−707.
(34) Yoganandan, G.; Balaraju, J. N.; William Grips, V. K. The Surface and Electrochemical Analysis of Permanganate Based Conversion Coating on Alclad and Unclad 2024 Alloy. *Appl. Surf. Sci.* **2012**, *258*, 8880−8888.
(35) Nguyen, T. D.; Dinh, C. T.; Do, T. O. Two-Phase Synthesis of Colloidal Annular-Shaped $Ce_xLa_{1-x}CO_3OH$ Nanoarchitectures Assemblied from Small Particles and Their Thermal Conversion to Derived Mixed Oxides. *Inorg. Chem.* **2011**, *50*, 1309−1320.
(36) Alexander, M. R.; Payan, S.; Duc, T. M. Interfacial Interactions of Plasma-Polymerized Acrylic Acid and an Oxidized Aluminium Surface Investigated Using XPS, FTIR and Poly(acrylic acid) as a Model Compound. *Surf. Interface Anal.* **1998**, *26*, 961−973.
(37) Kloprogge, J. T.; Duong, L. V.; Wood, B. J.; Frost, R. L. XPS Study of the Major Minerals in Bauxite: Gibbsite, Bayerite and (Pseudo-)Boehmite. *J. Colloid Interface Sci.* **2006**, *296*, 572−576.
(38) Huang, X.; Li, N. Structural Characterization and Properties of Lanthanum Film as Chromate Replacement for Tinplate. *Appl. Surf. Sci.* **2007**, *254*, 1463−1470.
(39) Zhang, X.; Zhang, P.; Wu, Z.; Zhang, Z. Facile Fabrication of Stable Superhydrophobic Films on Aluminum Substrates. *J. Mater. Sci.* **2012**, *47*, 2757−2762.
(40) Jafari, R.; Menini, R.; Farzaneh, M. Superhydrophobic and Icephobic Surfaces Prepared by RF-Sputtered Polytetrafluoroethylene Coatings. *Appl. Surf. Sci.* **2010**, *257*, 1540−1543.
(41) Castanho, S. M.; Moreno, R.; Fierro, J. L. G. Influence of Process Conditions on the Surface Oxidation of Silicon Nitride Green Compacts. *J. Mater. Sci.* **1997**, *32*, 157−162.
(42) Xu, W.; Liu, H.; Lu, S.; Xi, J.; Wang, Y. Fabrication of Superhydrophobic Surfaces with Hierarchical Structure through a Solution-Immersion Process on Copper and Galvanized Iron Substrates. *Langmuir* **2008**, *24*, 10895−10900.
(43) Xu, Q. F.; Wang, J. N.; Sanderson, K. D. Organic-Inorganic Composite Nanocoatings with Superhydrophobicity, Good Transparency, and Thermal Stability. *ACS Nano* **2010**, *4*, 2201−2209.
(44) Zhu, Y.; Zhao, Q.; Zhang, Y. H.; Wu, G. Hydrothermal Synthesis of Protective Coating on Magnesium Alloy using De-ionized Water. *Surf. Coat. Technol.* **2012**, *206*, 2961−2966.
(45) Zheng, J.; Bao, S.; Guo, Y.; Jin, P. Natural Hydrophobicity and Reversible Wettability Conversion of Flat Anatase TiO_2 Thin Film. *ACS Appl. Mater. Interfaces* **2014**, *6*, 1351−1355.
(46) Argyris, D.; Ashby, P. D.; Striolo, A. Structure and Orientation of Interfacial Water Determine Atomic Force Microscopy Results: Insights from Molecular Dynamics Simulations. *ACS Nano* **2011**, *5*, 2215−2223.

DOI: 10.1021/am505582j
ACS Appl. Mater. Interfaces 2015, 7, 1449−1457